Sequential deposition and metastable states in rare-earth/Co films

D. J. Webb and R. G. Walmsley*
Center for Materials Research, Stanford University, Stanford, California 94305

K. Parvin
Department of Physics, San Jose State University, San Jose, California 95192

P. H. Dickinson, T. H. Geballe, and R. M. White†
Department of Applied Physics, Stanford University, Stanford, California 94305
(Received 4 March 1985)

A study of the structural and magnetic properties of sequentially deposited (multilayered) sputtered films of Gd and Co is presented. It is found that by varying the deposition temperature, the film composition, and the multilayer sequences the film morphology can be controlled in a continuous way and, thus, new magnetic structures achieved. In particular, samples deposited at ambient temperature (80 °C) show clear evidence of layering and have fairly simple magnetic properties. On the other hand, at elevated deposition temperature (380 °C) no evidence of layers is seen, but one finds a pronounced chemical reaction which results in the formation of $GdCo_2$ in all cases where the nominal composition is on the Co-rich side of $GdCo_2$. It is demonstrated that one can take advantage of this reaction and use the multilayer sequences to control extrinsic properties of the films such as coercivity.

I. INTRODUCTION

The magnetic properties of matter may be separated into those which are intrinsic and those which are extrinsic. The intrinsic properties are quantum mechanical, or atomic, in origin, such as the saturation moment, the Curie temperature, magnetic anisotropy, etc. Extrinsic properties, such as the remanent magnetization, the coercivity, etc., also depend upon morphology—grain size, texture, and shape. These structural aspects are, in turn, governed by the preparation process. In this paper we present a study of multilayered films made by magnetron sputtering of alternating layers of rare earth (usually Gd) and Co. We find that the magnetic properties can be controlled in interesting ways by choice of deposition parameters.

The development of rapid-quench techniques for producing amorphous and other forms of nonequilibrium structures launched broad new studies.[1] In particular, vapor-phase techniques make it possible to control the composition of materials on an atomic scale as well as the morphology and, thus, make it possible to control a large variety of intrinsic and extrinsic properties. The control is best illustrated by the successes of molecular-beam epitaxy (MBE) in producing semiconductor heterostructures with novel properties.[2] Vapor deposition by electron beam and sputtering offers the possibility of extending some of the advantages of MBE in controlling composition and morphology to high melting temperature materials which are not easily evaporated from a cell.[3–6] The fact that the sputtered species generally arrive at the substrate with several volts of energy makes it difficult to achieve an atomically sharp interface when a more stable interface can be reached by diffusion. Thus, it is difficult to "engineer" interfaces with novel exchange interactions or to study the magnetic proximity effect, both of which phenomena involve characteristic lengths of the order a few atomic spacings. However, compositional modulation and multilayering can have a dramatic effect on the extrinsic magnetic properties. In particular, one might expect that new metastable states might be produced with unique properties which could be easily "tuned" to desired values through adjustment of the deposition parameters. Indeed, this is precisely what we find.

II. SAMPLE PREPARATION

The compositionally modulated films were sputtered in the vacuum system shown schematically in Fig. 1. The system was cryopumped to less than 1×10^{-6} Torr. The Gd source was then turned on, a thin film of Gd was deposited with the substrate protected, and the system was getter-pumped to around 5×10^{-7} Torr. During deposition the partial pressures of reactive gases in the neighbor-

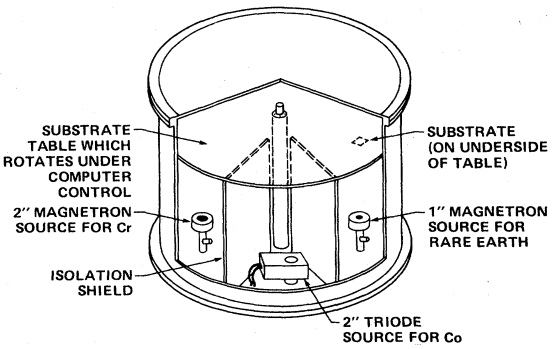

FIG. 1. Schematic representation of the sputtering chamber used in the deposition of multilayered samples.

hood of the sources was certainly much lower due to the gettering action of the large area of deposited material surrounding the substrate. This conclusion is born out by microprobe analysis of the films which shows no evidence (<1 at. %) of incorporated oxygen.

In the system configuration, the sources sputter up onto the substrates. The Co source was a 2-in. plasmax triode with a 99.99 + % pure Co target. The Gd source was a 1-in. planar magnetron whose target was arcmelted from a 99.9% pure Gd rod. The Cr source, used for the adhesion and protective layers, was a 2-in. planar magnetron source with a 99.99% pure Cr target. The substrates [Si (100) and (111) and sapphire ($1\bar{1}02$)] were chemically cleaned prior to placing them in the vacuum chamber. Then, ≈ 50 Å of Cr was deposited as an adhesion layer. The substrates were then positioned alternately over the Gd and Co sources to yield the desired compositional modulation. Finally, ≈ 50 Å of Cr was deposited to protect the sample from oxidation. For the Rutherford backscattering (RBS) measurements Al was used instead of Cr because of the mass difference between Al and Co.

Two methods of moving the substrates were tried. (1) The substrates were mounted on a rotating table; the sputtering rates of the Co and Gd sources and the speed of rotation were chosen so that each complete revolution resulted in a wavelength of modulation. The temperature of the substrates during deposition was not controllable when using this table, but was found to rise from 20 °C to about 90 °C. In this work, this deposition "temperature" is referred to as ambient. (2) The substrates were mounted on a Cu block on the end of an arm that could be alternately positioned over one source or the other. It was then easy to install a heater and control (to ± 5 °C) the temperature of the block, and thus the deposition temperature between 100 and 450 °C. The motion of this arm was determined using a computer-controlled stepping motor. The arm was kept over the source until the desired thickness was deposited; then, it was moved to the next source. The temperature of the Cu block was monitored using a chromel-alumel thermocouple.

The rate of deposition for each material was determined by running the source for a fixed time, and measuring the thickness of the deposit using a step profiler. In both cases the total thickness of the multilayer film was in good agreement with that expected from the measured rates of the two sources. The films were also analyzed for composition using an electron microprobe. The average composition of each film discussed in this paper is very close ($\pm 1\%$) to the composition estimated from the known thicknesses and bulk densities of each material. This value does not vary measurably over the surface of the film. Unless explicitly stated, we denote the particular multilayer film by "(number of bilayers)$\times$[(Gd thickness)/(Co thickness)]." Hence, 200 bilayers consisting of 100 Å Gd and 70 Å Co each is denoted by $200\times(100/70)$.

III. STRUCTURAL CHARACTERIZATION

The x-ray diffraction (XRD) results discussed in this paper were obtained using a modified Picker powder diffractometer which included an Eulerian cradle. Samples were mounted on a two-circle goniometer head allowing accurate adjustment of sample position. The radiation source was a Cu x-ray tube; the detection system was a bent graphite monochromator and proportional detector with pulse-height discrimination. The diffractometer was fully automated with all data acquired by a fixed-time-step scan mode. Fourier analysis of low-angle XRD data in order to obtain the periodic composition profile[3,6] was not done. In order to estimate the composition profile, RBS measurements[7] were carried out on a model system using specially prepared bilayers of Gd or Tb and Co. Terbium was used along with Gd because of convenience and the expectation that it is representative of all the heavy lanthanides in forming interfaces with Co. We used 2.2-MeV alpha particles and measured the backscattered flux simultaneously at 170° and 97° with solid-state detectors. In order to reduce the background, the beam was channeled through the single-crystal sapphire or silicon substrate. The instrumental broadening is estimated to be approximately a Gaussian with a full width at half maximum (FWHM) of 20 keV and was deconvolved from the data in order to clarify the details of the interface.

A. Ambient deposition temperature

1. X-ray diffraction

The high-angle (2θ above 10 degrees) diffraction results for Gd-Co samples deposited near ambient temperature are shown in Fig. 2. The first thing that is apparent in these data is that these samples, as deposited, are extremely disordered. The first peak in the scan for the 20/20 sample is extremely broad (FWHM greater than 12°), in fact, much broader than would be expected even for an

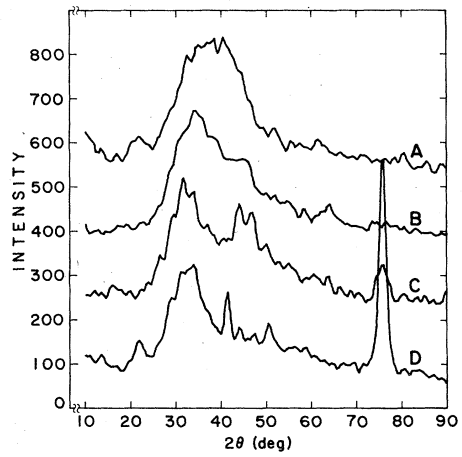

FIG. 2. X-ray intensity (Cu $K\alpha$ radiation) as a function of 2θ for several of the ambient deposition temperature samples. For clarity the curves have been arbitrarily offset in the vertical direction. In the present notation [(number of layers)$\times$(Gd layer thickness)/Co layer thickness)] the samples are *A*, $300\times(21/21)$; *B*, $152\times(37/37)$; *C*, $76\times(67/67)$; and *D*, $43\times(94/94)$. Peaks near 42°, 51°, and 76° are evidence for crystalline Co in the thickest bilayer samples.

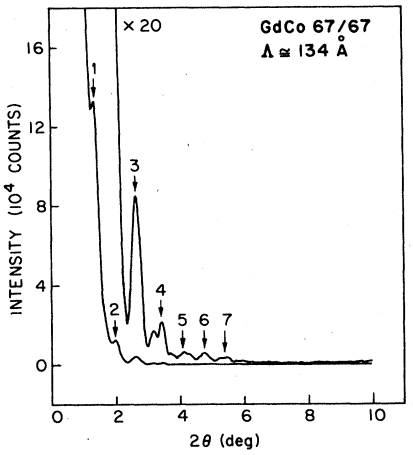

FIG. 3. X-ray intensity as a function of 2θ at low angles, showing Bragg scattering from the artificial layered structure in the $76\times(67/67)$ sample prepared at ambient temperature. Note also the "extra" structure between the expected third and fourth peaks.

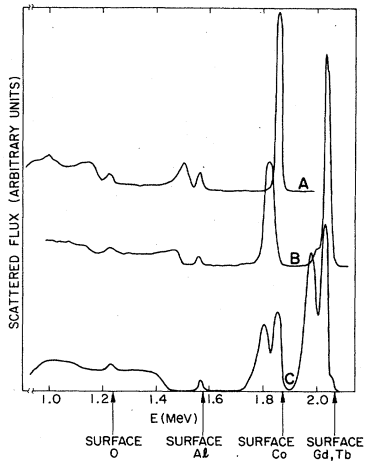

FIG. 4. Scattered flux as a function of α-particle energy for grazing exit angle (97°). Shown are the results of RBS runs on *A*, a Co standard (30 Å thick); *B*, a bilayer consisting of 30 Å Tb on 30 Å Co; and *C*, a film consisting of two bilayers of 40 Å Co on 40 Å Gd each. Each film was capped with 15 Å Al. The arrows indicate the energies where one would expect to see scattered flux from the respective elements if they were at the surface of the film.

amorphous structure of uniform composition.[8] As the bilayer period increases, this apparent single broad halo, divides into two broad halos with FWHM values for each halo more consistent with a uniform composition. At bilayer periods greater than 134 Å, evidence for microcrystalline Co is manifest. In fact, both hcp Co and fcc Co may be present.

Evidence from low angle (< 10 degrees) x-ray diffraction, an example of which is shown in Fig. 3, definitively demonstrated that although structurely highly disordered, the samples were nonetheless highly ordered compositionally in the direction of growth. The apparent first through seventh orders are marked in the figure. Since all Fourier components are present, the composition wave is not a simple sine or square wave. It is uncommon in metallic multilayers to find either of those two special cases. Of special note are the apparent reflections between the Fourier components of the expected modulation. These peaks indicate a periodicity, parallel to the growth direction, larger than that of the evident bilayer period. It may be that the composition wave has a longer (or shorter) period structure in it giving an unusual electron distribution in the sample. Another possibility is that this is a charge-density wave, perhaps initiated by the layering. This aspect is under further study.

From the XRD results it can be concluded that films prepared by sequential deposition of these elements are compositionally modulated amorphous structures at the shorter bilayer periods with the amplitude of the composition wave increasing with increasing bilayer period. At longer bilayer periods, evidence for crystalline hcp Co as well as fcc Co is observed.

2. *Rutherford Backscattering*

Rutherford backscattering measurements were carried out on several different samples. First, two standards were made of 30 Å Co and 30 Å Tb, respectively. Then, model films consisting of one, two, or three bilayers of thicknesses between 60 and 100 Å were made. In order to minimize the effects of oxidation of the films, each was capped with 15 Å Al. In this way we study each of the interfaces which will be found in a multilayer film.

In Fig. 4 we show the backscattered flux at 97° (exit angle of 7° from the sample plane), after correction for instrumental broadening for a one-bilayer film, a two-bilayer film, and the Co standard. We note that the Co standard as well as the Tb standard (not shown) yield simple results consisting of *symmetric peaks* at the appropriate energies. Since the data for the bilayers do not consist of symmetric peaks it is clear that the effects of the interface are seen.

In Rutherford backscattering the energy of the backscattered α particles is controlled by two effects. The rough energy scale is set by the mass of the scattering particle. A heavier nucleus (Tb) will scatter the He nuclei into larger final energy than will lighter nuclei (Co, Al, O). The finer details of the energy scale are determined by the inelastic He-electron scattering events through which the α particle loses energy as it moves through the film. Since this energy loss depends on the distance over which the α particle loses energy and the material through which it masses, it is easy to see that this technique can be a sensitive probe of interfaces. In practice, detector resolution, energy straggling, and substrate roughness generally limit the ultimate depth resolution to 10—30 Å.[9]

One immediately sees from Fig. 4 that the two interfaces are qualitatively the same. For Tb on Co the Tb peak has a small shoulder on the low-energy side, indicating diffusion of a relatively small amount of Tb into Co. The Co peak here is broader than that of the Co standard but without much asymmetry. Although an explanation based on a fine-scale surface roughening is possible, we think it is more likely that the interface results from sim-

ple diffusion of a small portion of the Tb into the Co giving an interface which is Co rich and 20—30 Å wide. The other interface is displayed in the bottom spectrum. One sees that there is a small shoulder on the high-energy side of the highest-energy Gd peak. This is very similar to the low-energy shoulder seen in the middle spectrum. We thus conclude broadly that the two types of interface in a multilayer film of rare-earth/Co are not sharp but consist of a Co-rich region of 20—30 Å.

B. Elevated deposition temperature

As is evident in Fig. 5, 380 °C was sufficient to ensure crystallinity at all bilayer periods but insufficient to achieve a high degree of crystalline perfection or interfacial coherence. In fact, low-angle diffraction results provide no evidence for compositional modulation. Such lack of low-angle scattering does not imply that no order remains but rather that the amplitude and/or coherence of any remaining composition wave was insufficient to produce detectable coherent scattering. For clarity we will continue to refer the samples in terms of their "bilayer period." For these elevated deposition temperature samples, though, a more correct term is probably "deposition period."

The currently accepted phase diagram for the Gd-Co system[9] specifies $GdCo_3$ as the stable phase at the average composition of the symmetric multilayer films. That is, an equal thickness bilayer contains three times as many Co atoms as Gd atoms. Interestingly, no evidence for the $GdCo_3$ phase was found in any of the multilayer films, even for those annealed to 500 °C after deposition. The only intermetallic phase which XRD detected was $GdCo_2$, a cubic Laves phase[10] of the structure type $MgCu_2$. The probable explanation for the absence of $GdCo_3$ is a kinetic preference for $GdCo_2$ in these highly nonequilibrium films. It is also possible, although not probable, that the low-temperature portion of the phase diagram is in error. Often, kinetic sluggishness at low temperatures make the establishment of equilibrium difficult and high-temperature data is arbitrarily extrapolated to low temperatures. If $GdCo_2$ were nucleating from a homogeneous matrix, the latter explanation would take on more relevance. However, since the composition range dynamically available during deposition spans the phase diagram, the kinetic explanation is considered more likely.

Upon examining the diffraction information in Fig. 5 more closely, a number of trends may be noted. First, at the smaller bilayer period, only $GdCo_2$ is conclusively in evidence. Concomitantly, with an increase in the bilayer period, peaks near those expected for both hcp and fcc Co begin to appear. The proximity of the deposition temperature (380 °C) to the Co hcp←fcc transition temperature (420 °C) would make the coexistence of the two structures not unexpected. Further trends with increasing bilayer period include an increase in the coherence length for (220) stacking of $GdCo_2$ in the growth direction and a shift toward smaller (220) spacings.

After correction for instrumental broadening, the FWHM of the (220) reflection was translated by the Debye-Scherrer equation into average particle size and is shown in Fig. 6. The assumption inherent in the application of the Debye-Scherrer equation, that broadening is only due to grain-size effects, is certainly an oversimplification. However, as an indicator of the effect of bilayer period on coherence length in the growth direction, the application may be justified. Since the coherence length scales with the bilayer period for small bilayers, the grain size evidently does likewise. The lack of a similar correlation for larger bilayers indicates that grain sizes are limited by diffusion. Comparing the diffraction patterns for the layered structures (*A*, *B*, and *C* of Fig. 5) with that for the compound $GdCo_2$ deposited at the same temperature (*D* in Fig. 5), the effect on grain size (or, more broadly, crystalline order) is apparent.

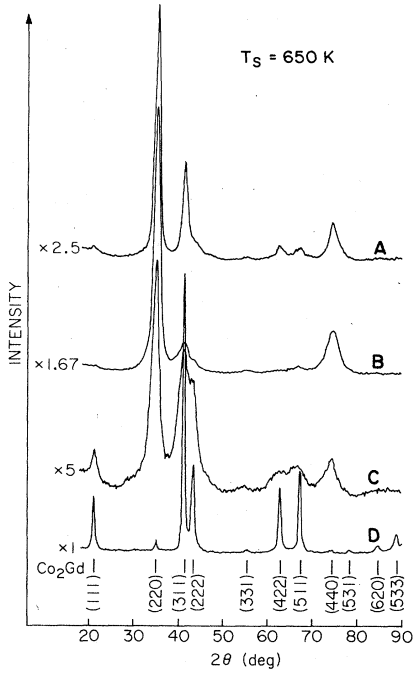

FIG. 5. X-ray intensity (Cu $K\alpha$ radiation) as a function of 2θ for several of the high-deposition temperature samples. Data are for *A*, 50×(100/100); *B*, 165×(30/30); *C*, 250×(20/20); and *D*, a homogeneous $GdCo_2$ film also deposited at 380 °C. The positions of the Bragg reflections for the $GdCo_2$ Laves phase are also marked.

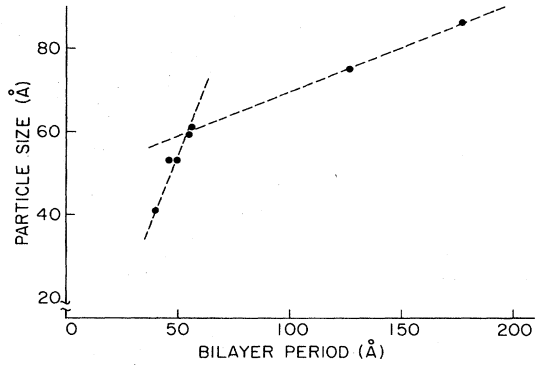

FIG. 6. Grain size (Debye-Sherrer) estimated from XRD as a function of the bilayer period.

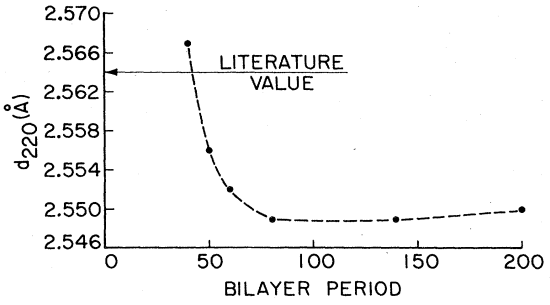

FIG. 7. $GdCo_2$ (220) d spacing from XRD as a function of the bilayer period.

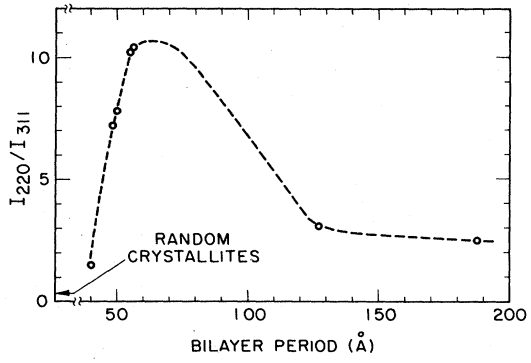

FIG. 8. Ratio of the intensities of the (220) and (311) reflections as a function of the bilayer period.

The systematic shift of the (220) spacing with bilayer period is shown in Fig. 7. The strong (220) texture of these films prevented accurate determination of the lattice spacing shifts for other reflections except for shifts of the (440) spacing which were consistent with that for the (220) spacing. Origins for such lattice parameter shifts include uniform strain and stoichiometric variation. Strain may be uniform on a macroscopic scale such as bulk residual film stresses or microscopic, such as interfacial stresses which, for these films, would likely be periodic throughout the film thickness. The strains consistent with the lattice parameter shifts observed would correspond to stresses well beyond reasonable expectations for a yield stress. Hence, if strain is the origin of the shift in lattice parameter, it must be a periodic interfacial microstrain.

In principle it is possible to differentiate between volume distortions such as stoichiometry variations might induce and lineal distortions such as microstrain by examining different reciprocal directions in the film with the x-ray scattering vector. This procedure entails rotating the sample about the goniometer axis so that the scattering vector lies at some angle to the film normal. Unfortunately, diffraction results at 45° to the film normal were inconclusive. The strong texture of the microcrystalline, highly disordered films made measurements of the (220) lattice spacing near normal incidence practical, but at 45° from normal, reflections were of insufficient intensity to accurately determine peak positions.

As noted above and seen in Fig. 5, several of the films showed a strong (220) texture. It also appears that the texture changes as a function of the bilayer period. As a qualitative measure of the texture we use the intensity of the (220) reflection, I_{220}, scaled by the intensity of the (311) reflection, I_{311}. This ratio is plotted in Fig. 8 as a function of the bilayer period. The intermediate bilayer period samples are seen to be strongly textured with the (220) planes stacked in the plane of the film while the smallest and largest bilayers have crystallites apparently approaching random orientation (noted in the figure). The results of this change of texture and crystal size (Fig. 6) will be seen below in the bilayer period dependence of the coercive field.

In summary, XRD results show that a pronounced reaction takes place in these films when prepared at 380 °C. The compound $GdCo_2$ is formed, and no evidence of compositional modulation is seen. Since these films have a net composition equal to $GdCo_3$ there must also be Co (or very Co-rich) regions separating the $GdCo_2$ grains. In addition, the grain size and film texture are apparently controlled by the deposition period (bilayer thickness).

IV. MAGNETIC MEASUREMENTS

The magnetization measurements were made with a standard (PAR 155) vibrating-sample magnetometer. A Janis SuperVaritemp cryostat was used to control the temperature for measurements between 4 and 300 K. The temperature in this range was monitored with a Cu-Constantan thermocouple. Above room temperature a PAR 153 oven was used and the temperature was measured with a Chromel-Alumel thermocouple. The magnetic field was chosen to be parallel ($H_{||}$) or perpendicular ($H_{\perp}$) to the film and was swept between 0 and ±19 kOe.

A. Ambient deposition temperature

First we discuss samples prepared at ambient temperature. An example of a hysteresis loop for one of these films is shown in Fig. 9. Each of these samples had a room-temperature coercivity less than 50 Oe in the parallel and perpendicular directions. When the temperature was decreased to 4 K, no significant change in the coercivities was observed. The small value of H_c is not surprising when one considers the high-angle x-ray dif-

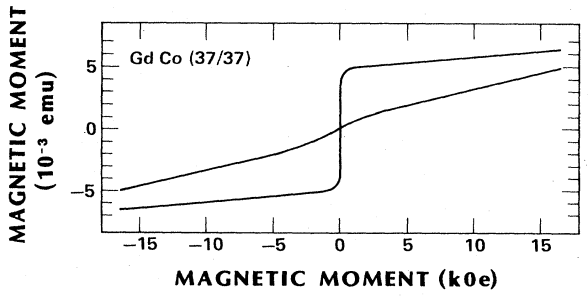

FIG. 9. Hysteresis loops with field oriented parallel or perpendicular to the sample plane for GdCo 152×(37/37) layers deposited at ambient temperature.

fraction measurements which showed that these alloys consist only of regions which are amorphous or very small-grained crystalline (see also Refs. 11 and 12).

As we have pointed out earlier, from a stoichiometry point of view, the average composition of a symmetric bilayer sample is equivalent to that of a $GdCo_3$ alloy. Thus, in order to present our magnetization results in a transparent form, we calculate the moment per formula unit of $GdCo_3$ from the measured values of the saturation magnetization at 4.2 K (Table I). Except for the $43\times(94/94)$ sample the magnetizations of our multilayered films are very close to that reported[13] for homogeneous crystalline $GdCo_3$ ($2.3\mu_B$ per formula unit). In $GdCo_3$ the Gd has its full moment ($7\mu_B$) aligned parallel to the field, and all of the Co moments are antiparallel. We therefore conclude that the same is true for our modulated films, even though the Gd and Co are clearly not uniformly mixed, indicating that the predominant exchange interactions are ferromagnetic for Gd-Gd and Co-Co and antiferromagnetic for Gd-Co.

To make this point clearer we have calculated Co moments as follows. We have assumed that at 4 K all Gd moments are ordered and are parallel to the applied field with the value $7\mu_B$ per atom. Using this value and our measured value of the film moment, we estimate the moment associated with each cobalt atom. Table I shows the result. A negative value implies that the net Co moment is antiparallel to the Gd moment.

For small bilayer thickness (40—70 Å) almost all the available Co atoms have their moments antiparallel to the Gd moments, resulting in the average atomic cobalt moment of $\approx 1.5\mu_B$ which is close to that of bulk Co ($1.7\mu_B$).[14] Figure 10 shows schematically a typical GdCo multilayer prepared at ambient temperature with the directions of moments with respect to H indicated.

As the bilayer thickness is increased (70—200 Å), the magnitude of the cobalt moment opposite to the gadolinium moment is decreased. The XRD and RBS data lead to the conclusion that there are layers of pure Co in these large bilayer films. Thus, the decrease in the Co moment shown in Table I is associated with the existence of some pure cobalt at the center of the layer with corresponding moment turned toward the applied field. We speculate that when the bilayer thickness is increased further (>200 Å), isolated grains of Co form which are free to orient themselves parallel to the field.

As seen in Fig. 9, at 4 and 300 K a field applied perpendicular to the film does not saturate the magnetization even at the highest field tried (19 kOe). In contrast, $M_{\|}$ (magnetization with field applied parallel to the film surface) saturates above a few hundred oersted. This indicates a high degree of in-plane anisotropy which is not unusual in films of rare-earth/Co.[15]

TABLE I. Magnetic moments of samples prepared at ambient temperature.

Sample	μ per $GdCo_3$ (μ_B)	estimated μ per Co (μ_B)
$300\times(21/21)$	2.2	−1.6
$152\times(37/37)$	2.7	−1.4
$43\times(94/94)$	4.3	−0.9

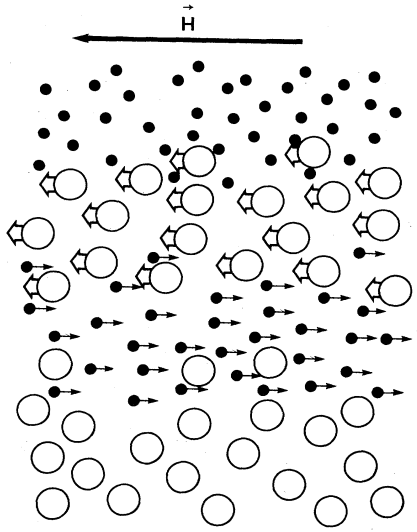

FIG. 10. Schematic representation of Gd and Co moments in a multilayer film deposited at ambient temperature.

B. Elevated deposition temperature

Samples prepared at the substrate temperature of 380 °C have high coercivities in the parallel direction which vary between 500 and 5000 Oe with *no significant difference* between the values obtained at 4 and 300 K. Such a wide range of coercive force has also been observed in amorphous GdCo films by Cuomo *et al.*[16] In that case the coercive field was changed by changing composition and thus moving the compensation point with respect to room temperature, resulting in a coercive field (near room temperature) which had a strong T dependence. Here the coercive fields unexpectedly do not depend on T and so are not due to proximity to a compensation point. Figure 11 shows the dependence of H_c on symmetric bilayer thickness measured at 4 and 300 K. It is seen that H_c increases rapidly to the maximum value of 5000 Oe as the bilayer thickness is increased from 40 to 80 Å. Beyond the maximum point H_c decreases slowly. Comparison of Fig. 11 with the XRD results shown in Figs. 6 and 7 suggests a mechanism responsible for this bilayer dependence

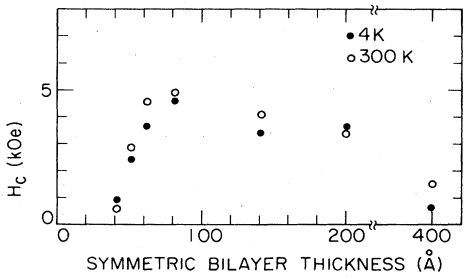

FIG. 11. Coercive field as a function of bilayer period for several of the samples deposited at 380 °C. Compare with Figs. 6 and 8.

TABLE II. Magnetic moments for samples prepared at elevated temperature.

Sample	μ per $GdCo_3$ (μ_B) 4 K	μ per $GdCo_3$ (μ_B) 300 K	estimated μ per $GdCo_2$ (μ_B) 4 K	estimated μ per $GdCo_2$ (μ_B) 300 K
250×(20/20)	3.3	1.5	5.0	3.2
200×(25/25)	2.9	1.5	4.6	3.2
165×(30/30)	2.3	1.0	4.0	2.7
70×(70/70)	2.4	1.2	4.1	2.9
50×(100/100)	2.2	1.3	3.9	3.0
25×(200/200)	8.1	2.0	9.8	3.7

of coercivity. The low value of H_c (500 Oe) for a 250×(20/20) sample is associated with the small grain sizes which XRD shows to be randomly oriented (Fig. 8). As the grain size is increased H_c increases indicating that it becomes more difficult either to nucleate or to reorient magnetic domains. For much larger grain sizes (samples with bilayer periods greater than 200 Å) the effects of grain-boundary pinning are less important in determining H_c. One might suspect from such an explanation that the films with the smallest grain size would show evidence of superparamagnetism. No clear evidence of this effect was observed, although there are suggestions in the data for the 40-Å bilayer sample that samples with lower thicknesses might be superparamagnetic. On the other hand, these small grains are not isolated but are probably strongly coupled to their neighbors. In this case one would not expect to see simple superparamagnetic behavior.

When the measuring field is applied perpendicular to the sample plane one finds that H_c at 300 K is about 400 Oe for 250×(20/20) and 200×(25/25) films. Since we cannot saturate the magnetization in the larger bilayer period samples in 19 kOe, we cannot get a reliable estimate of H_c. Amorphous $GdCo_3$ films are known to have a vertical orientation when deposited in special ways[16,17] (for instance with substrate bias), so it is not surprising that in our most homogeneous and most disordered films there is some indication of a vertical orientation. Decreasing the temperature to 4 K does not change these coercivities dramatically.

Since the low-angle XRD does not show any evidence of modulation, and since the existence of $GdCo_2$ crystallites with disordered cobalt have been verified by high-angle XRD, we analyze our magnetization data assuming the film consists of a mixture of $GdCo_2$ and Co. As before, we first calculate the moment per formula unit of $GdCo_3$. Then, assuming the cobalt moments ($1.7\mu_B$) are antiferromagnetically coupled to $GdCo_2$ moments, we estimate the moment of $GdCo_2$. Such an opposite alignment of Gd and Co moments seems to be the norm[13,16,17] in uniform GdCo films. Except for one case, the resulting values for the $GdCo_2$ moment (Table II) turn out to be between $4.0\mu_B$ and $4.6\mu_B$ at 4 K and between $2.7\mu_B$ and $3.3\mu_B$ at 300 K.

We have also made a homogeneous film of $GdCo_2$ where we find that the moment per $GdCo_2$ formula unit is $4.7\mu_B$ at 4 K and $3\mu_B$ at 300 K. The discrepancy between this value and the estimated magnetic moment of $GdCo_2$ in the multilayer is probably due to the lack of complete alignment of $GdCo_2$ moments with the external field due to the orientational spread (Fig. 6) of easy axes of the crystallites. In the case of the 25×(200/200) sample we get an unusually large deduced value for the $GdCo_2$ moment ($9.8\mu_B$ at 4 K and $3.7\mu_B$ at 300 K) which, as in the 50×(94/94) ambient deposition temperature films, indicates that some of the Co is aligning with the field. This inhomogeneous ordering is also seen in the hysteresis loops. The samples with deposition periods (bilayers) greater than 140 Å have hysteresis loops made up of a low-coercive-field component (presumably Co) and a larger coercive-field component (presumably large-grain $GdCo_2$).

To verify the postulate of antiferromagnetic coupling of Co and $GdCo_2$ moments, we have measured remanent magnetic moment versus temperature from 300 to 600 K (shown in Fig. 12). In each sample a ferrimagnetic type of behavior with an apparent compensation temperature (T_{comp}) is observed. Table III gives the results of this measurement.

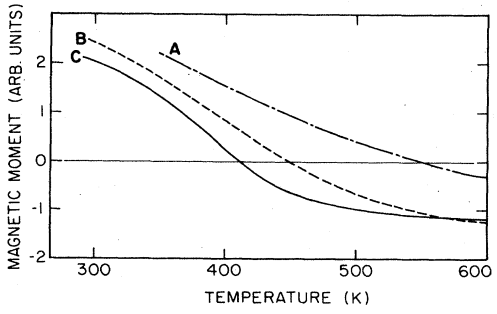

FIG. 12. Remanent magnetization as a function of temperature for GdCo samples deposited at 380°C. The samples shown are *A*, 250×(20/20); *B*, 70×(70/70); and *C*, 25×(200/200).

TABLE III. Compensation temperatures for films made at elevated temperature.

Sample	T_{comp} (K)
250×(20/20)	550
200×(25/25)	505
165×(30/30)	497
70×(70/70)	447
50×(100/100)	435
25×(200/200)	410

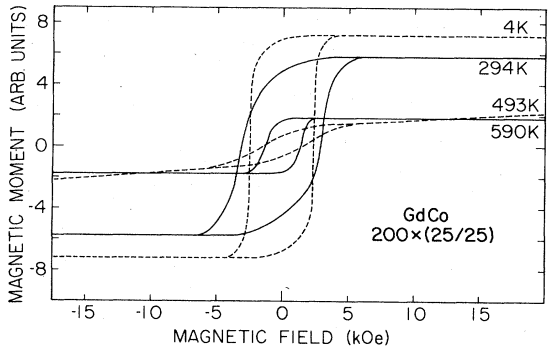

FIG. 13. Hysteresis loops at several temperatures for GdCo 200×(25/25). Note that the loop shape changes near T_{comp} but that the loop width does not diverge.

The fact that each sample exhibits a compensation point substantiates our assumption regarding the antiferromagnetic coupling of $GdCo_2$ and Co moments. We note, however, that this is not a compensation point in the normal sense. For a homogeneous ferrimagnet one finds that the coercive field diverges at the compensation temperature since the crystalline anisotropy is proportional to M^{-1}.[18] Although measurements near T_{comp} are difficult to make because M is very small, it appears that for these multilayer films the coercive field does not diverge near T_{comp}, Fig. 13. Instead, as the temperature is increased through T_{comp} the hysteresis loop changes its shape (two components to the magnetization are exhibited) and just above T_{comp} the loop is actually narrower than the low-temperature loops. To explain these results we suggest that the moment due to the $GdCo_2$ decreases toward 0 as T is increased toward T_{comp} and the moment due to the excess Co begins to turn with the applied field. Thus, at temperatures lower than T_{comp} the remanent magnetic moment is due to difference in moments of Co and $GdCo_2$ and at temperatures larger than T_{comp} the magnetic moment is dominated by the Co and stays nonzero up to the Curie temperature of Co.

Within the above picture there is also a natural explanation for the deposition period (bilayer thickness) dependence of T_{comp}. Our picture implies that the compensation point is determined by (slightly lower than) the temperature at which the $GdCo_2$ moment vanishes. Therefore, the relevant temperatures where M goes to zero are the Curie transition for crystalline $GdCo_2$, $T_c \simeq 400$ K, and the compensation temperature for amorphous (highly disordered) $GdCo_2$, $T_{comp} \simeq 510$ K. As noted earlier, XRD data show that the $GdCo_2$ present in the film becomes more disordered (both in terms of grain size and orientation) as the bilayer period is decreased. Thus, as the bilayer period decreases one expects that the $GdCo_2$ moment will disappear (and oppositely oriented Co moment becomes manifest) at progressively higher T. Hence, T_{comp} increases as seen in Table III. Note that the total moment left well above T_{comp} is roughly independent of bilayer thickness.

V. CONCLUSIONS

We have found that the deposition temperature, the composition, and the multilayer sequences are all important variables which can be varied independently to give different compositional structures and, thus, to give different magnetic structures. At ambient deposition temperature, sequential deposition of Gd and Co results in a compositionally modulated structure. The RBS data imply that there are asymmetric interface regions, each of about 20—30 Å, separating Co and Gd layers. Magnetization measurements have shown that the Gd moments are antialigned with the Co moments except for the thickest bilayers where the Co begins to turn toward an applied field.

At moderate deposition temperatures a pronounced chemical reaction occurs which results in the formation of $GdCo_2$ in all cases where the nominal composition is on the Co-rich side of $GdCo_2$. In all such cases the resulting composite consists of $GdCo_2$ and Co. The $GdCo_2$ grain size correlates with the amount of element deposited in each period. Thus, one has essentially continuous control of grain size as well as achieving a fairly uniform grain size over the bulk of the sample.

As a result of this control of the morphology one can "tune" the extrinsic magnetic properties such as coercive field, compensation temperature (not usually thought of as an extrinsic property), and total moment of a film through wide ranges of values. In particular, without changing the net composition of a film we are able to adjust the coercive field between 5 and 5000 Oe by simply altering the deposition parameters. The coercive field thus achieved does not depend on the proximity to a compensation point but is actually independent of temperature over a wide range of T. In addition, each of these parameters can be modified by changing the film composition.

We believe that this method of controlling the growth parameters in a film has great generality and depends mostly on the kinetics of the alloy system for the formation of a particular (nonequilibrium) compound. Analogous results have also been obtained when Tb is substituted for Gd. This suggests that in general the formation of the Laves-phase (RCo_2) compound may be the kinetically favored reaction at the rare-earth/Co interface. This further suggests that there is a high probability of obtaining very sharp interfaces in multilayered RCo_2/Co films.

ACKNOWLEDGMENTS

One of us (K.P.) would like to thank Professor Ingolf Lindau for his interest in this work. Part of this work was done while K. Parvin was at Stanford Synchrotron Radiation Laboratory which is supported by the Department of Energy, Office of Basic Energy Research. He would also like to acknowledge partial support from Associated Western Universities, Inc. Some of the magnetization measurements were made at Xerox Palo Alto Research Center and we are grateful to the staff for their help and hospitality. We also thank Professor T. Sigmon for useful discussions regarding the Rutherford backscattering technique. This work was supported in part by NSF Grant No. DMR-8313295 and also by the IBM Corporation.

*Present address: H. P. Laboratories, Building 25, 3500 Deer Creek Rd., Palo Alto, CA 94304.

†Also at Control Data Corporation, Box O-HQSO8A, 3100 34th Ave. S., Minneapolis, MN 55440.

[1]For a recent review see K. Moorjani and J. M. D. Coey, *Magnetic Glasses* (Elsevier, Amsterdam, 1984).

[2]For a review of MBE and significant results see Venkatesh Narayanamurti, Phys. Today **37**(**10**), 24 (1984).

[3]For reviews of the structural aspects of multilayered films see Charles M. Falco, Wayne R. Bennett, and Ahmed Boufelfel, in *Dynamical Phenomena at Surfaces, Interfaces, and Superlattices* (Springer, New York, in press); D. B. McWhan, in *Synthetic Modulated Structure Materials,* edited by Leroy Chang and W. C. Giessen (Academic, New York, 1984).

[4]S. Ruggiero, T. W. Barbee, and M. R. Beasley, Phys. Rev. Lett. **45**, 1299 (1980).

[5]Robert Walmsley, Joyce Thompson, Daniel Friedman, Robert M. White, and Theodore H. Geballe, IEEE Trans. Magn. **MAG-19**, 1992 (1983).

[6]D. B. McWhan, M. Gurvitch, J. M. Rowell, and L. R. Walker, J. Appl. Phys. **54**, 3886 (1983).

[7]For a review of Rutherford backscattering techniques see W. K. Chu, J. W. Mayer, M. A. Nicolet, G. Amsel, T. Buck, and F. Eisen, Thin Solid Films **17**, 1 (1973).

[8]R. G. Walmsley, A. F. Marshall, D. Bouchet, and D. A. Stevenson, J. Non-Cryst. Solids **54**, 277 (1983).

[9]J. S. Williams and W. Möller, Nucl. Instrum. Methods **156**, 213 (1978).

[10]K. H. J. Buschow and A. S. Van der Goot, J. Less-Common Met. **17**, 249 (1969).

[11]Rodney P. Elliot, in *Proceedings of the Fourth Conference on Rare Earth Research,* edited by LeRoy Eyring (Gordon and Breach, New York, 1964).

[12]T. Chen, D. A. Rogowski, and R. M. White, J. Appl. Phys. **49**, 1816 (1978).

[13]E. Burzo, Phys. Rev. B **6**, 2882 (1972).

[14]A. H. Morrisch, *The Physical Principles of Magnetism* (Wiley, New York, 1965), p. 270.

[15]R. Walmsley, K. Parvin, R. M. White, and T. H. Geballe (unpublished).

[16]J. J. Cuomo, P. Chaudhari, and R. J. Gambino, J. Electron, Mater. **3**, 517 (1974); P. Chaudari, J. J. Cuomo, and R. J. Gambino, Appl. Phys. Lett. **22**, 337 (1973).

[17]R. Hasegawa, J. Appl. Phys. **45**, 3109 (1974).

[18]A. H. Morrisch, *The Physical Principles of Magnetism* (Wiley, New York, 1965), p. 350.